# Observations of Recirculation in the Bore Fluid During Hollow Fiber Spinning

**Y. Su and G. G. Lipscomb**
Chemical and Environmental Engineering Dept., University of Toledo, Toledo, OH 43606

**H. Balasubramanian and D. R. Lloyd**
Chemical Engineering Dept., University of Texas, Austin, TX 78712

*DOI 10.1002/aic.10830*
*Published online March 27, 2006 in Wiley InterScience (www.interscience.wiley.com).*

*Hollow fiber membranes are used widely in membrane separation processes because of their high surface area to volume ratio. Several models have been developed for the hollow fiber spinning process. However, many details of the process are not well understood. In this work, the conservation of mass and momentum equations are solved for isothermal, axisymmetric hollow fiber spinning. In contrast to past work, the conservation equations are solved for both the bore and clad fluids. The two sets of equations are linked by continuity of velocity and stress across the bore–clad interface. Simulation results show an unexpected recirculation region in the bore fluid under certain operating conditions. For a given die geometry, the presence/absence and size of the recirculation region is dependent on the bore-to-clad flow rate ratio and bore-to-clad viscosity ratio. The appearance of the recirculation region leads to a more rapid decrease of both fiber outer and inner radii after die swell. The predicted changes in fiber radii are in better agreement with experimental observations than predictions from the one-dimensional thin filament analysis.* © 2006 American Institute of Chemical Engineers *AIChE J,* 52: 2072–2078, 2006
*Keywords: hollow fiber membrane, fiber spinning, fluid mechanics*

## Introduction

Membrane separation processes are used in a variety of industries from water treatment to industrial gas separations. These processes commonly use polymeric membranes in flat sheet or hollow fiber form. The hollow fiber form is widely used because of its high surface area to volume ratio and is the preferred form in ultrafiltration, dialysis, and gas separation processes.

Hollow fiber spinning processes may be categorized as melt or solution spinning based on the type of spin dope. Solution processes use a polymer solution with one or more solvents, while melt processes use the neat polymer. Additionally, spinning processes may be categorized as dry, wet, or dry–wet processes based on the type of quench used. Dry processes use a gas to quench the extrudate, wet processes use a liquid quench, and dry–wet processes use both a gas and a liquid quench. These processes are described in more detail in the literature.[1]

Commonly, the hollow fiber spinning process is divided into four regions along the axial direction for analysis, as shown in Figure 1. The bore (inner) and clad (outer) fluids are in fully developed shear flow inside the spinneret in region 1. After exiting the spinneret, the flow rearranges quickly from shear to elongational flow in region 2. Die swell usually accompanies this transition. The fiber is drawn down to the desired final size and quenched in the draw zone (region 3). After cooling to the glass transition or crystallization temperature, the nascent membrane solidifies in the solidification region (region 4), which limits further dimensional changes.

Correspondence concerning this article should be addressed to G. G. Lipscomb at glenn.lipscomb@utoledo.edu.

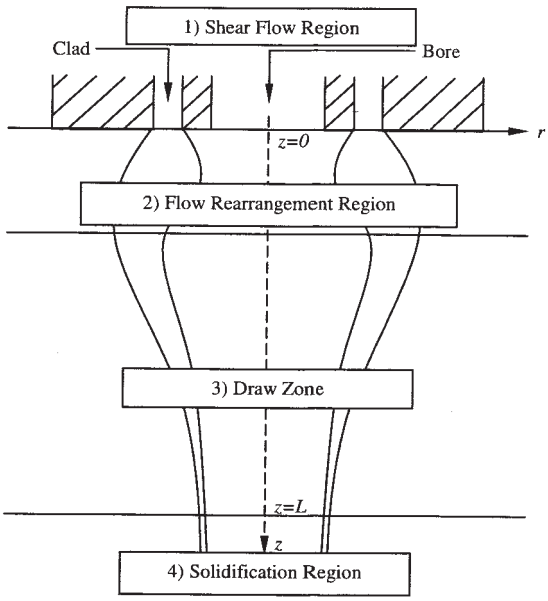


**Figure 1. Hollow fiber spinning regions.**

The first models of hollow fiber spinning were one-dimensional models that describe the changes that occur in the draw zone region only. Freeman et al.,[2] Lipscomb,[1] Chung et al.,[3] De Rovére and Shambaugh,[4] and Balasubramanian[5] developed these models based on thin filament analysis (TFA). TFA was developed originally for solid fiber spinning and simplifies the governing conservation equations to a set of ordinary differential equations through radial averaging or, equivalently, by assuming the axial velocity is a function of axial position in the draw zone only.

Recent work describes the development of (2-D) models. Freeman et al.[2] and Oh et al.[6] report 2-D simulations of the melt hollow fiber spinning process, while Berghmans et al.[7] and Batarseh[8] report simulations of the solution spinning process. Unfortunately, the last three models neglect the transition region and examine transport in the draw zone only. Freeman et al. include the transition region but do not include transport in the bore fluid; the bore fluid is replaced by the assumption of a constant pressure at the bore–clad interface.

In this work, the governing conservation equations are solved in the shear flow, flow rearrangement, and draw zone regions for both the bore and clad fluids. The results show an unexpected recirculation region in the bore fluid under certain conditions. Additionally, the filament size decreases more rapidly along the draw zone than predicted by the 1-D TFA, which is consistent with experimental observations.

## Model Development

### *Model equations and assumptions*

Isothermal, melt spinning is considered here. Energy and mass transfer are not included in the analysis. Thus, only the continuity and momentum conservation equations are solved for both the bore and clad regions subject to the following assumptions:

(1) The bore is concentric with the clad so the geometry is axisymmetric.

(2) The spinning process is steady-state.

(3) Stress induced crystallization does not occur in the draw zone.

(4) Both bore and clad fluids are incompressible Newtonian fluids.

(5) No slip occurs at the bore–clad interface.

(6) Air drag, gravity, and surface tension are negligible.

One would expect the assumption of a Newtonian clad fluid to be valid for sufficiently low die shear rates and draw zone elongation rates. Moreover, results for Newtonian fluids provide a basis for interpreting non-Newtonian effects. The assumption of a constant density bore fluid is expected to be valid for a bore gas based on past thin filament analyses.[2] This work indicates bore gas pressure changes are small, of order magnitude 10 kPa, so pressure related density changes should be small.

The governing continuity and momentum conservation equations for the bore and clad are:

$$\nabla \cdot \underline{v}_i = 0 \tag{1}$$

$$\rho_i \underline{v}_i \cdot \nabla \underline{v}_i = -\nabla p_i + \eta_i \nabla^2 \underline{v}_i \tag{2}$$

where the subscript $i$ is either $b$ to represent the bore fluid or $c$ to represent the clad.

### *Boundary conditions*

To predict die swell, the fluid computational domain must extend inside the spinneret to a point where the shear flow is fully developed, as illustrated in Figure 2. The boundary conditions that apply at this inlet boundary are:

$$v_{z,b} = \frac{2Q_b}{\pi R_{bo}^2}\left(1 - \left(\frac{r}{R_{bo}}\right)^2\right) \tag{3a}$$

$$v_{z,c} = \frac{2Q_c}{\pi R_{co}^2}\left(\frac{\ln(1/\kappa)}{\ln(1/\kappa)(1-\kappa^4) - (1-\kappa^2)^2}\right) \times \left(1 - \left(\frac{r}{R_{co}}\right)^2 + \left(\frac{1-\kappa^2}{\ln(1/\kappa)}\right)\ln\left(\frac{r}{R_{co}}\right)\right) \tag{3b}$$

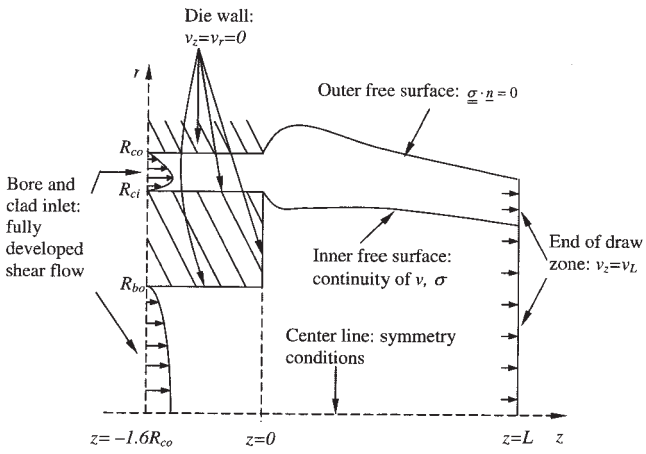


**Figure 2. Computational domain and boundary conditions.**

**Table 1. Base Spinning Conditions**

| Condition | Value |
|---|---|
| $R_{co}$ = spinneret clad outer radius | $1.9 \times 10^{-3}$ m |
| $R_{ci}$ = spinneret clad inner radius | $1.55 \times 10^{-3}$ m |
| $R_{bo}$ = spinneret bore outer radius | $9.0 \times 10^{-4}$ m |
| $Q_c$ = clad volumetric flow rate | 15.82 cc/min |
| $Q_b$ = bore volumetric flow rate | 1.00 sccm (1.51 ccm @ $T^0$, $p_b^0$) |
| $T^0$ = spinning temperature | 413 K |
| $p_b^0$ = initial bore gauge pressure | 58 Pa |
| $v_L$ = take-up velocity | 35 m/min |
| $L$ = draw zone length | 0.20 m |
| $p_{atm}$ = ambient air pressure | 101325 Pa |

$$v_{r,i} = 0 \tag{3c}$$

where $Q$ is the volumetric flow rate and $\kappa = R_{ci}/R_{co}$. The axial location of the inlet boundary (that is, the value of $z$ associated with the inlet) is arbitrary, but the inlet region must be sufficiently long that the predicted velocity and diameter profiles do not depend on it. Simulations with varying values for the inlet indicate setting $z = -1.6R_{co}$ satisfies this requirement.

Boundary conditions at the end of the draw zone, $z = L$, are:

$$v_{z,i} = v_L \tag{4}$$

where $v_L$ is the specified takeup velocity that determines the final fiber size. One might consider a zero normal stress boundary condition for the bore fluid, but the nature of large scale spinning operations suggests Eq. 4 is the proper boundary condition. Commonly, large quantities of fiber are accumulated as one continuous filament on a spool for use in membrane module production. If the bore fluid does not move with the same velocity as the clad at the end of the draw zone, and thereafter in the accumulated fiber, a pressure gradient must exist along the entire length of the filament. Given the operating pressures (typically, steady bore feed pressures are less than 1 kPa gauge, see Table 1), there is insufficient pressure difference to drive the bore fluid through such a length of fiber. During startup, the accumulated lengths will be much shorter and one might consider use of a zero normal stress boundary condition. However, during steady spinning, the accumulated length will be sufficiently long to eliminate pressure driven flow.

Symmetry along the center line of the computational domain leads to the following boundary conditions for $r = 0$:

$$v_{r,b} = \frac{\partial v_{z,b}}{\partial r} = 0 \tag{5}$$

No slip along the die wall requires that:

$$v_{r,i} = v_{z,i} = 0 \tag{6}$$

Along the fiber outer surface, one may set the normal and tangential forces to zero if viscous forces exerted by the quench gas are small and surface tension is negligible:

$$\underline{\underline{\sigma}}_c \cdot \underline{n}_o = 0 \tag{7}$$

where $\underline{n}_o$ is the unit normal to the outer surface and $\underline{\underline{\sigma}}$ is the fluid stress tensor. For an incompressible Newtonian fluid, the stress tensor is given by:

$$\underline{\underline{\sigma}}_i = \eta_i(\nabla \underline{v}_i + (\nabla \underline{v}_i)^T) - p_i \underline{\underline{I}} \tag{8}$$

where $\eta$ is the fluid viscosity and $\underline{\underline{I}}$ is the unit tensor. Along the bore–clad interface, continuity of the velocity and equality of the normal and tangential forces lead to the following boundary conditions:

$$\underline{\underline{\sigma}}_b \cdot \underline{n}_i = \underline{\underline{\sigma}}_c \cdot \underline{n}_i \tag{9a}$$

$$\underline{v}_b = \underline{v}_c \tag{9b}$$

where $\underline{n}_i$ is the unit normal to the bore–clad interface.

At steady state, the inner and outer fluid interfaces are stationary. Therefore, the velocity normal to each interface is zero and explicitly setting the velocity equal to zero yields an equation that determines the location of the interface. Along the outer interface, setting the normal velocity to zero gives:

$$v_{z,c} \frac{\partial R_{co}}{\partial z} - v_{r,c} = 0 \tag{10}$$

while along the inner interface the result is:

$$v_{z,c} \frac{\partial R_{ci}}{\partial z} - v_{r,c} = v_{z,b} \frac{\partial R_{ci}}{\partial z} - v_{r,b} = 0 \tag{11}$$

Note that the inner interface is pinned at the die surface at $r = R_{ci}$ while the outer interface is pinned at $r = R_{co}$. Both interfaces are not free to travel along the die surface. In spinning operations, the spin dope ideally does not wet the surface of the die, that is, it does not spread along the die surface and displace either the bore fluid or the external quench fluid that contacts the die. Wetting of the surface would interfere with the ability to produce fibers of a uniform, desired size and is avoided in commercial spinning processes. Therefore, pinning the two interfaces is consistent with industrial experience.

## Spinning System and Numerical Approximation of Governing Equations

The results presented here are for a polyethylene–dodecanol dry–wet, solution spinning process using a nitrogen bore gas. The base spinning conditions and material properties summarized in Tables 1 and 2 correspond to a system reported in the literature for which experimental measurements of fiber size in the draw zone are available.[5]

This experimental system is not strictly isothermal. The spin dope is extruded at 413 K and passes through an air quench at room temperature before entering a chilled water quench bath. Upon entering the water bath, the filament cools rapidly and undergoes a phase transition that leads to solidification.

Experimental measurements of the filament temperature and predictions from a thin filament analysis of the draw zone indicate the temperature change in the draw zone is small, less than 10 K. Therefore, to a first approximation, the draw zone is nearly isothermal. Additionally, solvent evaporation is small, so a comparison between experimental fiber size measurements and the simulation results reported here is appropriate.

**Table 2. Polyethylene-Dodecanol System Material Properties**

| Property | Value |
|---|---|
| $\rho_c$ = clad density | 758 kg/m$^3$ |
| $\eta_c^0$ = pre-exponential factor for clad shear viscosity | $6.07 \times 10^{-3}$ Pa s |
| $E_c/R_g$ = ratio of activation energy to the gas constant for clad shear viscosity | 3681 K |
| $\eta_b$ = bore gas shear viscosity at spinning temperature | $0.22 \times 10^{-4}$ Pa s |
| $MW$ = bore gas molecular weight | 28.0 |

The clad Newtonian viscosity is calculated for a given spinning temperature from an Arrhenius relationship:

$$\eta_c = \eta_c^0 \exp\left(\frac{E_c}{R_g T}\right) \tag{12}$$

where $\eta_c^0$ is the pre–exponential factor and $E_c$ is the activation energy. Values for the parameters were determined experimentally using a commercial rheometer.[5] The clad density and bore gas viscosity were estimated a priori from the literature.

Numerical approximations to the solution of the governing conservation equations were obtained using the commercial computational fluid dynamics program FIDAP (Fluent Inc.). FIDAP uses the finite element method (FEM) to reduce the governing partial differential equations to a set of algebraic equations. This reduction requires discretizing the solution domain into a finite number of polygonal regions using a mesh. A typical mesh is illustrated in Figure 3. Mesh refinement studies (doubling or tripling the number of elements) suggest the predicted fiber dimensions are accurate to within 5%.

Initially, the location of the free surface is unknown and is guessed; the initial mesh shown in Figure 3 assumes the free surface location is independent of axial position. The radial positions of nodal points on free surfaces (relative to a reference base line, such as the center line) are introduced as additional solution variables. These variables are determined simultaneously with the pressure and velocity field to satisfy the kinematic boundary conditions of Eqs. 10 and 11. Detailed descriptions of the free surface tracing technique and solution algorithm are provided in the FIDAP user manual.[9] Figure 3 also illustrates a typical final mesh for the solutions reported here.

## Results and Discussion

### *Solid fiber spinning*

To test the use of FIDAP to solve free surface problems, results were obtained for solid fiber spinning. To simulate solid fiber spinning, the spinneret clad inner radius was set equal to zero ($R_{ci} = 0$) and the boundary conditions at the bore-clad interface (Eqs. 9 and 11) were not used; instead, the boundary conditions along the fiber centerline were given by Eq. 5 upon substituting the clad velocity for the bore velocity. The predicted value of die swell (maximum filament diameter/die diameter) is in excellent agreement with past work; the calculated value is 1.126 while literature values[10-14] range from 1.126 to 1.131, with the most recent work reporting a value of 1.1265.[14] Additionally, changes in fiber size and velocity in the draw zone are in excellent agreement with predictions of the thin filament analysis.

### *Free annular jet*

To further test FIDAP, the die swell of a free annular jet of a Newtonian fluid was simulated by replacing the fixed velocity at $z = L$ with a zero axial velocity gradient and omitting the bore fluid region from the computational domain. For a die with $R_{co}/R_{ci} = 1.23$, the calculated increases of 6.1% and 2.1% for the outer and inner radii, respectively, are nearly identical to the values of 5.5% and 1.6% reported in the literature[12] for a die with $R_{co}/R_{ci} = 1.33$. The differences are most likely due to different mesh resolutions and the slight differences in die geometry. Moreover, at these mesh resolutions, the numerical values for the radii are accurate to ~1%, that is, the location of the outer surface is accurate to three significant figures and differences less than 1% are not significant.

### *Hollow fiber spinning*

The simulation results provide values for fiber size along the draw zone and values for the radial and axial velocity components throughout the solution domain. These results are presented in two forms here: (1) streamline and (2) axial velocity contour plots. The streamline plots allow visualization of fluid flow paths, while the axial velocity plots allow visualization of the flow rearrangement region and velocity changes in the

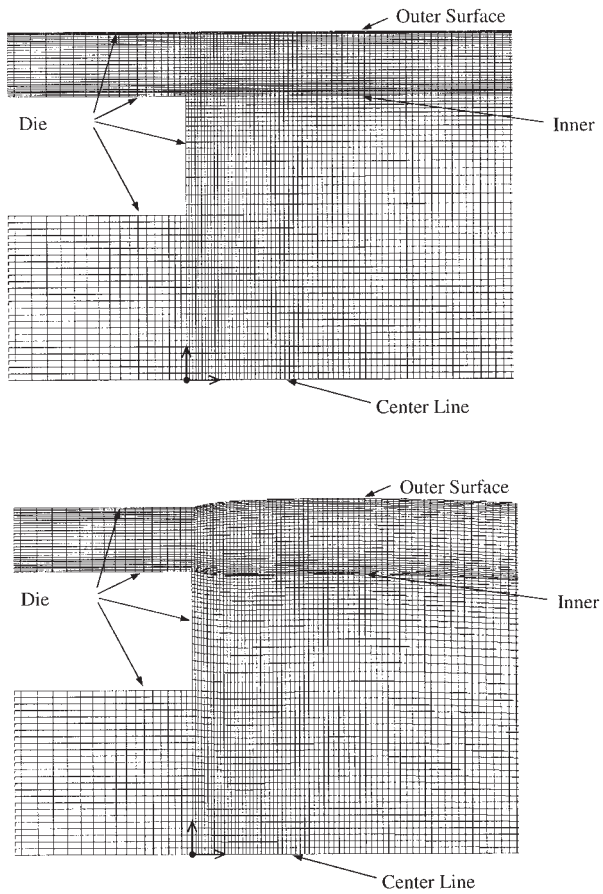


**Figure 3. Typical meshes used in the simulations: original mesh (top) and final mesh (bottom).**

Note that only the portion of the mesh closest to the die is shown. The origin of the axisymmetric coordinate system is indicated by the two arrows along the center line.

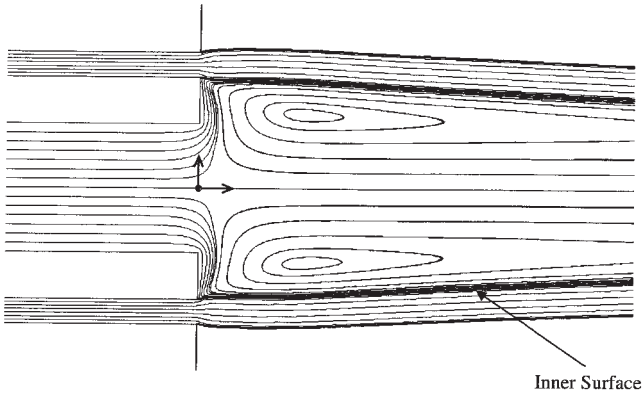


**Figure 4. Typical streamline contour plot showing flow near the die exit.**

The arrows indicate the origin of the coordinate system.

process. Figure 4 illustrates the computed fluid streamlines for the base conditions given in Tables 1 and 2, while Figure 5 illustrates the axial velocity contours. Note that a complete cross-section of the filament is shown in Figures 4 and 5 as opposed to half of the cross-section as shown in Figures 2 and 3. Additionally, only that portion of the results closest to the die are shown since this is the region of greatest interest.

Figures 4 and 5 clearly show the primary characteristics of the spinning processes. The shear field in the spinneret quickly rearranges to an elongational flow in the transition region and is accompanied by die swell. The elongational flow in the draw zone leads to draw down of the fiber to the desired size.

Surprisingly, Figures 4 and 5 also show a recirculation region exists in the bore. The region extends from the spinneret face a distance of $\sim 0.4\ L$. The presence of this region impacts the filament diameter and how it changes along the draw zone. This in turn will impact heat and mass transfer to the surrounding quench air. Additionally, the recirculation will impact any mass transfer that occurs between the bore and clad fluids.

For a fixed spinneret geometry and low speed (that is, inertialess) spinning conditions, the simulation results depend on two dimensionless groups: (1) $\eta_b/\eta_c$ and (2) $Q_b/Q_c$. Simulations were run over a wide range of values for these parameters to determine when recirculation occurs.

Figure 6 illustrates the effect of changing the viscosity ratio for a fixed flow rate ratio of 0.095 (=1.51/15.82). Above a critical viscosity ratio of 0.15, the recirculation region is absent. As the viscosity ratio decreases below this critical value, a recirculation region emerges and grows in size.

The recirculation region appears as the bore fluid expands to fill the interior of the extruded filament, resulting in a decrease in the bulk bore velocity. This velocity reduction is superimposed on a velocity increase at the bore–clad interface due to no-slip at the interface. The simultaneous bulk velocity decrease and interfacial velocity increase generates large shearing stresses in the transition region. For sufficiently high viscosities, the bore fluid is able to withstand this shearing. However, for low viscosities, the shearing results in the generation of a recirculation vortex. In isothermal spinning, the gauge bore pressure always decreases in magnitude along the draw zone.[1] Thus, if the initial gauge bore pressure is negative, the recirculation region may also be supported by a positive pressure gradient—an increasing absolute bore pressure with distance along the draw zone. However, this gradient is expected to be small as gauge bore pressures are typically less than 1 kPa in magnitude.

Similar results are found when the viscosity ratio is held constant and the flow ratio is changed. Above a critical flow rate ratio, recirculation does not occur. As the flow ratio is decreased below the critical value, a recirculation region appears and grows in size.

Simulation results for the $\eta_b/\eta_c$ and $Q_b/Q_c$ ranges examined are summarized in Figure 7. Figure 7 indicates which combinations of values result in recirculation and the size of the recirculation region expressed as $L_{rec}$(recirculation zone length)/$L$. Recirculation occurs only for combinations that lie below a critical line. As either ratio decreases, the recirculation region increases in size. For example, for a fixed bore-to-clad flow rate ($Q_b/Q_c \sim 0.1$), the length of the recirculation region increases from $0.05L$ when the viscosity ratio is $10^{-3}$ to $0.4L$ when the viscosity ratio is $5 \times 10^{-7}$.

When a gas is used as the bore fluid, the viscous stress contribution to the bore fluid stress is small relative to the pressure contribution and may be neglected in the equation for the continuity of the stress across the bore–clad interface (Eq. 9a). Furthermore, the thin filament analysis suggests the bore gas pressure decreases upon expansion into the flow rearrangement region, but this decrease and subsequent changes along the draw zone are small. Therefore, one might expect similar predictions of fiber size and velocity if one omits the bore fluid domain in the simulation and replaces Eq. 9a with a constant pressure boundary condition along the bore–clad interface. The value for the pressure is adjusted to produce the desired final fiber size; note that the pressure replaces the bore flow rate as the parameter that controls size.

Figure 8 compares results from simulations *with and without* a bore fluid (the *without* simulations use the constant pressure boundary condition along the bore–clad interface). The calculated fiber dimensions are in excellent agreement. Thus, it appears one can predict fiber size without including the bore fluid domain. However, this will not allow simulation of bore fluid recirculation and its effect on heat and mass transfer.

Predictions of fiber inner and outer radii along the spinline are compared to the 1-D TFA predictions and experimental results[5] in

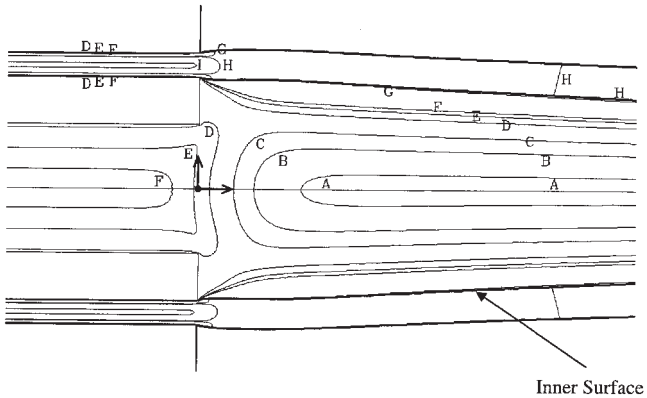


**Figure 5. Typical axial velocity contour plot showing flow near the die exit.**

A: −50, B: −35, C: −20, D: 2, E: 12, F: 18, G: 56, H: 60, I: 100 (mm/s). The arrows indicate the origin of the coordinate system.

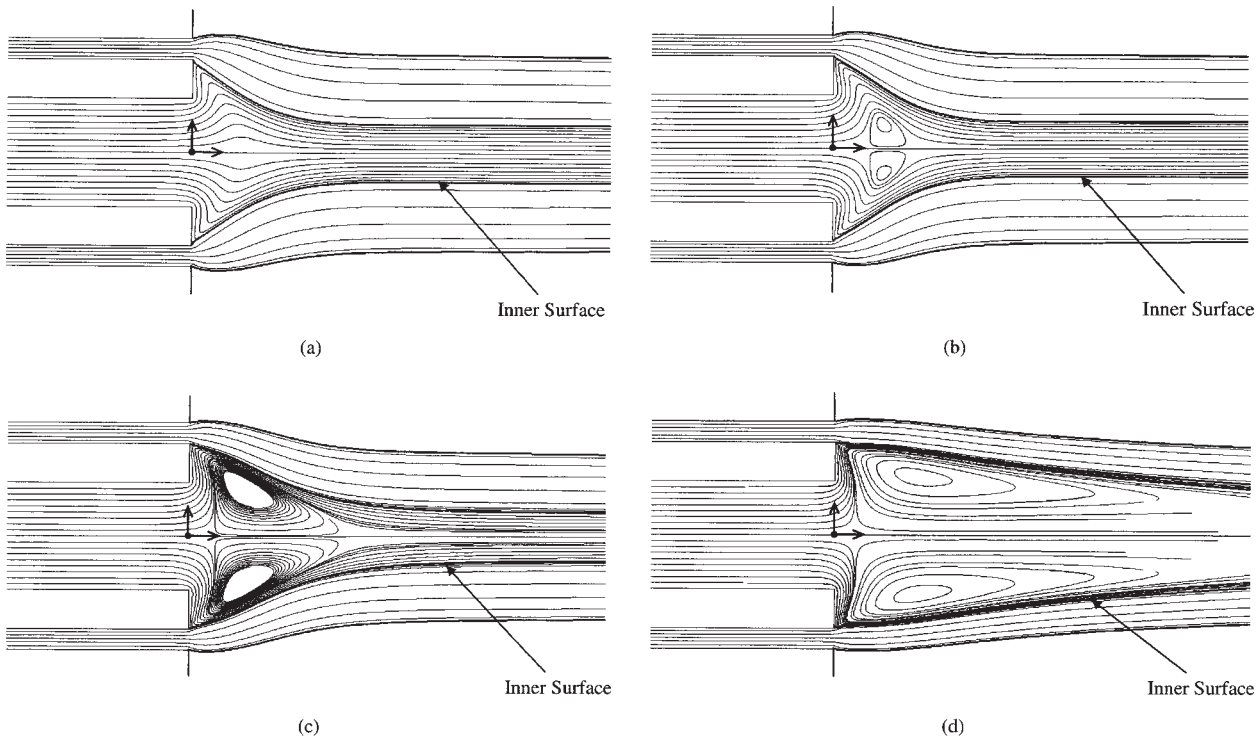


**Figure 6. Streamline contour plots near the die exit with same bore-to-clad flow rate ratio ($Q_b/Q_c$ = 0.095).**

(a) $\eta_b/\eta_c$ = 0.17, (b) $\eta_b/\eta_c$ = 0.1, (c) $\eta_b/\eta_c$ = 0.02, (d) $\eta_b/\eta_c = 2 \times 10^{-4}$. The arrows indicate the origin of the coordinate system.

Figure 9. Due to experimental limitations, measurements of the fiber inner radius are not available. For the TFA simulations, the maximum fiber diameter in the die swell region, obtained from the full 2-D simulation, was used as the initial outer radius and the initial inner radius was calculated from continuity using the given bore and clad flow rates.

The TFA predicts a much thicker fiber wall than the 2-D simulation near the spinneret. In this region, bore fluid recirculation increases the cross-sectional area occupied by the bore, which leads to a larger inner radius. The recirculation region vanishes at the point where the inner radii predicted by the 1- and 2-D simulations start to overlap.

Elimination of the recirculation region leads to a more rapid decrease in the fiber outer radius than predicted by the TFA. This improves the agreement between the experimental observations and the theoretical predictions. However, significant differences still exist between the predictions and experiments that the inclusion of non-Newtonian properties may resolve. Because the final fiber dimensions are determined by the feed flow rates and the take-up velocity, the 1- and 2-D calculations yield the same fiber radii at the end of the draw zone.

Figure 9 indicates the present work underestimates the maximum die swell in the transition region. This may be due to

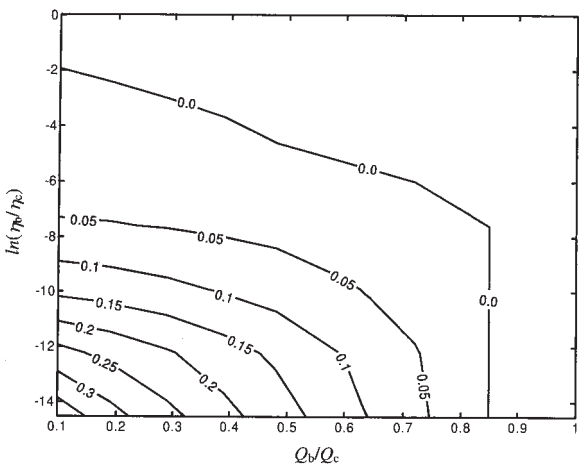


**Figure 7. Contour plot of $L_{rec}/L$ as a function of $\ln(\eta_b/\eta_c)$ and $Q_b/Q_c$.**

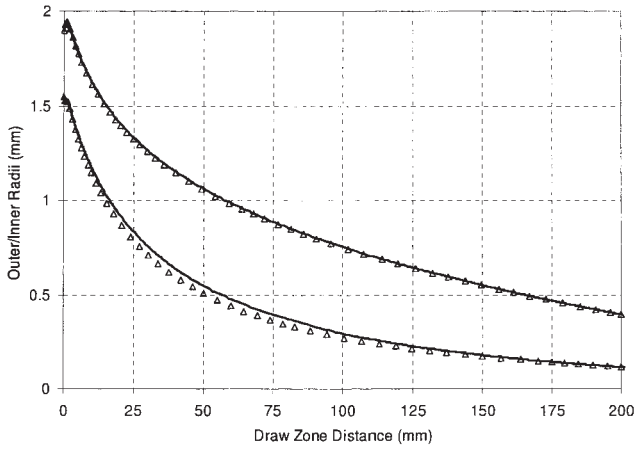


**Figure 8. Fiber radii along the spinline from simulations with (triangles) and without (solid lines) a bore fluid.**

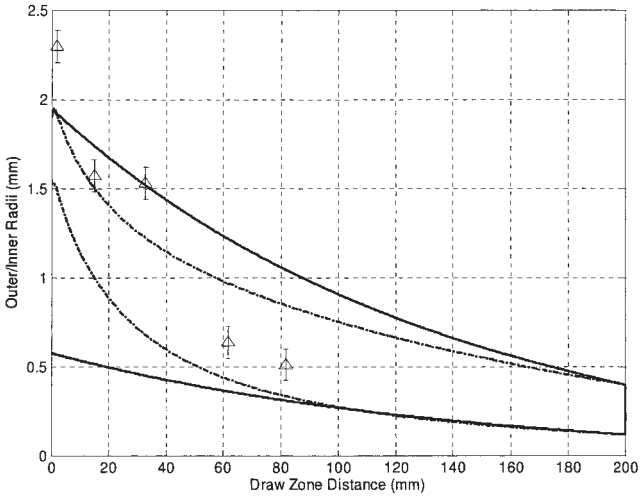


**Figure 9. Present work (dashed lines), TFA (solid lines), and experimental values (triangles) of fiber outer (upper curves) and inner radii (lower curves) along spinline; experimental values are for outer radius only.**

non-Newtonian fluid effects as well. The literature indicates that die swell can increase significantly with fluid elasticity, and such effects were not included in the work reported here.[10-14] However, use of an appropriate non-Newtonian fluid constitutive equation may improve the comparison.

## Conclusions

Simulations of the isothermal hollow fiber spinning process are presented that include both the bore and clad fluid domains. The results indicate that a recirculation region may appear in the bore fluid under certain conditions. The bore-to-clad flow rate and viscosity ratios are the key parameters that determine the presence/absence and the size of the recirculation region for a given die geometry.

The appearance of the recirculation region leads to a more rapid decrease in both inner and outer fiber radii along the draw zone than predicted by the one-dimensional model. This leads to better agreement with experimental observations of fiber outer radius. These differences in fiber dimensions may affect heat and mass transfer in the fiber and the concomitant development of membrane structure. Therefore, including the bore fluid region in the simulation domain may be critical in simulations of hollow fiber spinning for industrially relevant process conditions.

While solution of the full 2-D conservation equations will be required to determine die-swell of the clad, given the clad geometry one may be able to predict the existence and size of the recirculation zone using a lubrication analysis. Such an analysis is beyond the scope of the present work but might provide an analytical prediction of the existence of recirculation.

## Acknowledgments

This work was supported by the National Science Foundation.

## Notation

$E$ = viscosity activation energy (J/kmol)
$I$ = unit tensor
$L$ = draw zone length (m)
$L_{rec}$ = recirculation zone length (m)
$MW$ = molecular weight (kg/kmol)
$\underline{n}_i$ = unit normal to the bore–clad interface
$\underline{n}_o$ = unit normal to the outer surface
$P$ = pressure (Pa)
$P_{atm}$ = atmospheric pressure (Pa)
$Q$ = volumetric flow rate (cc/min)
$r$ = radial coordinate (m)
$R_{bo}$ = spinneret bore outer radius (m)
$R_{co}$ = spinneret clad outer radius (m)
$R_{ci}$ = spinneret clad inner radius (m)
$R_g$ = gas constant (J/kmol/K)
$T$ = spinning temperature (K)
$v$ = velocity (m/min)
$v_L$ = take-up velocity (m/min)
$z$ = axial coordinate (m)

### *Greek letters*

$\eta$ = Newtonian viscosity (Pa s)
$\kappa$ = radius ratio parameter ($=R_{ci}/R_{co}$)
$\rho$ = density (kg/m$^3$)
$\underline{\underline{\sigma}}$ = fluid stress tensor

### *Subscripts and superscripts*

$0$ = initial value
$b$ = bore fluid value
$c$ = clad fluid value
$i$ = bore or clad fluid
$r$ = radial coordinate value
$z$ = axial coordinate value

## Literature Cited

1. Lipscomb GG. The melt hollow fiber spinning process: steady-state behavior, sensitivity and stability. *Polymers for Advanced Technologies.* 1994;5:745-758.
2. Freeman BD, Denn MM, Keunings R, Molau GE, Ramos J. Profile development in drawn hollow tubes. *J Polym Eng.* 1986;6:171-186.
3. Chung T-S, Xu Z-L, Lin W. Fundamental understanding of the effect of air-gap distance on the fabrication of hollow fiber membranes. *J Appl Polym Sci.* 1999;72:379-395.
4. De Rovére A, Shambaugh RL. Melt-spun hollow fibers: modeling and experiments. *Polym Eng Sci.* 2001;41:1206-1219.
5. Balasubramanian HA. Dissertation, University of Texas at Austin, 2004.
6. Oh TH, Lee MS, Kim SY, Shim HJ. Studies on melt-spinning process of hollow fibers. *J Appl Polym Sci.* 1998;68:1209-1217.
7. Berghmans S, Berghmans H, Meijer HEH. Spinning of hollow porous fibers via the TIPS mechanism. *J Membr Sci.* 1996;116:171-189.
8. Batarseh MT. Dissertation, University of Texas at Austin, 1999.
9. FIDAP Theory Manual, Lebanon, NH: Fluent, Inc., 2002.
10. Nickell RE, Tanner RI, Caswell B. The solution of viscous incompressible jet and free-surface flows using finite-element methods. *J Fluid Mech.* 1974;65:189-206.
11. Crochet MJ, Keunings R. Die swell of a Maxwell fluid: numerical prediction. *J Non-Newtonian Fluid Mech.* 1980;7:199-212.
12. Caswell B, Viriyayuthakorn M. Finite element simulation of die swell for a Maxwell fluid. *J Non–Newtonian Fluid Mech.* 1983;12:13-29.
13. Tanner RI. *Engineering Rheology.* Oxford: Clarendon Press; 1985.
14. Georgiou GC, Boudouvis AG. Converged solutions of the Newtonian extrudate swell problem. *Int J Numer Methods Fluids.* 1999;29:363-371.

*Manuscript received Aug. 18, 2005, and revision received Feb. 7, 2006.*